NACA RM A53F22

RESEARCH MEMORANDUM

LIFT, DRAG, AND HINGE MOMENTS AT SUPERSONIC SPEEDS OF AN ALL-MOVABLE TRIANGULAR WING AND BODY COMBINATION

By William C. Drake

Ames Aeronautical Laboratory
Moffett Field, Calif.

NATIONAL ADVISORY COMMITTEE
FOR AERONAUTICS
WASHINGTON

September 16, 1953
Declassified August 12, 1958

NATIONAL ADVISORY COMMITTEE FOR AERONAUTICS

RESEARCH MEMORANDUM

LIFT, DRAG, AND HINGE MOMENTS AT SUPERSONIC SPEEDS OF AN ALL-MOVABLE TRIANGULAR WING AND BODY COMBINATION

By William C. Drake

SUMMARY

This report presents hinge-moment data for a wing-body combination at Mach numbers of 1.46 and 1.99; in addition, lift and drag results are also presented at the lower Mach number. The model tested consisted of an aspect ratio 4, triangular, all-movable wing with an 8-percent-thick double-wedge section mounted on a pointed cylindrical body of fineness ratio 9-1/3. At the lower Mach number, the test data cover an angle-of-attack range from about -6° to about 15° with wing deflections ranging from -5° to 16°; at the higher Mach number, the respective ranges are from about -5° to about 28° and 0° to 16°. Results of systematic tests made to determine the effects of Reynolds number, fixing transition on the body nose, and wing-body gap width are also presented.

The results contained in this report show that the triangular, all-movable wing has a relative effectiveness (defined as the ratio of experimental lift to theoretical lift) ranging from 63 to 98 percent. For equal angles, the lift and drag rise due to wing deflection are less than those due to model angle of attack. Since the maximum center-of-pressure shift was found to be only about 3 percent of the mean aerodynamic chord, the control can be fairly closely balanced over a large range of angles of attack and deflection at a Mach number of 1.46. The effects of the variations of Reynolds number and gap and of fixing transition on the body nose are shown to be negligible or small.

Comparisons are made between experiment and theory. The theories used are discussed and shown to be adequate within the ranges of angles of attack and deflections for which the theories are applicable.

INTRODUCTION

In a review of the literature for the preparation of reference 1, it was found that there were relatively little experimental supersonic data currently available on hinge moments of all-movable wings. It is the purpose of this report to present data for a body in combination with a triangular wing at Mach numbers of 1.46 and 1.99 and to compare the results with available theory.

SYMBOLS

A_p plan-form area of body, sq in.

C_D foredrag coefficient, $\frac{\text{total drag - base drag}}{qS_B}$

C_{D_o} foredrag coefficient when $\alpha = 0^\circ$ and $\delta = 0^\circ$

C_h hinge-moment coefficient, $\frac{\text{hinge moment}}{qS_B\bar{c}}$

C_{h_α} rate of change of hinge-moment coefficient with angle of attack, $\frac{\partial C_h}{\partial \alpha}$, per deg

C_L lift coefficient, $\frac{\text{lift}}{qS_B}$

C_{L_α} rate of change of lift coefficient with angle of attack, $\frac{\partial C_L}{\partial \alpha}$, per deg

$\bar{c}$ mean aerodynamic chord, $\frac{2}{3} c_r$, in.

c_{d_c} section drag coefficient for an infinite cylinder

c_r root chord of wing (at body juncture), in.

d body diameter, in.

g wing-body gap width (at $\delta = 0^\circ$), in.

K_N, $K_{B(W)}$, $k_{B(W)}$, $K_{W(B)}$, $k_{W(B)}$ — lift-ratio parameters for body nose, body in presence of wing, and wing in presence of body (See ref. 1 for complete definitions.)

M — Mach number

q — dynamic pressure, lb/sq in.

R — Reynolds number, based on body length

S_B — body cross-section area, sq in.

$\frac{\bar{x}}{c_r}$ — distance from leading edge of wing-body juncture to center of pressure of wing panel in fraction of wing root chord

$\left(\frac{x}{c_r}\right)_H$ — distance from leading edge of wing-body juncture to hinge line in fraction of root chord

$\frac{\bar{x}-x_H}{\bar{c}}$ — distance of center of pressure of the wing panel from the hinge line in fraction of mean aerodynamic chord

α — angle of attack, deg

$\alpha_{D_{min}}$ — angle of attack for minimum drag, deg

δ — wing deflection angle, deg

η — relative effectiveness of the wing in lift, $\frac{(C_L)_{exp}}{(C_L)_{theo}}$

$\bar{\eta}$ — correction to c_{d_c} for finite length

Subscripts

B(W) — body (exclusive of nose) in presence of wing

exp — experiment

H — hinge line

min — minimum

N	nose
nom	nominal
theo	theory
W	wing alone
W(B)	wing in presence of body
α	α variable, δ constant
δ	δ variable, α constant

Coefficients used without subscripts refer to the wing-body combination.

Figure 1 shows the positive sense of all coefficients, angles, and directions.

THEORETICAL CONSIDERATIONS

Lift

In reference 1 it was shown that the total lift of a body-wing combination is

$$C_L = \left\{ \left[K_N + K_{B(W)} + K_{W(B)} \right] \alpha + \left[k_{B(W)} + k_{W(B)} \right] \delta \right\} \left(C_{L_\alpha} \right)_W \qquad (1)$$

Equation (1) can be separated into its component parts: lift due to angle of attack

$$\Delta C_L = \left[K_N + K_{B(W)} + K_{W(B)} \right] \alpha \left(C_{L_\alpha} \right)_W \qquad (\delta \text{ constant}) \qquad (2)$$

and lift due to wing deflection

$$\Delta C_L = \left[k_{B(W)} + k_{W(B)} \right] \delta \left(C_{L_\alpha} \right)_W = K_{W(B)} \delta \left(C_{L_\alpha} \right)_W \qquad (\alpha \text{ constant}) \qquad (3)$$

Reference 1 stated that experimental values of $(C_{L_\alpha})_W$ should be used when available in preference to the value from linear theory. The experimental value of $(C_{L_\alpha})_W$ at M = 1.50 for a geometrically similar wing (ref. 2) was corrected to a Mach number of 1.46 and utilized in the calculations; its value is tabulated in table I. The value of $(C_{L_\alpha})_W$ from linear theory is about 15 percent higher than the experimental value. Also listed in table I are the various lift-ratio parameters (obtained from fig. 1 of ref. 1) required for equations (1), (2), or (3).

Drag

Drag due to lift is calculated from

$$C_D = C_{D_o} + \frac{1}{57.3}\left\{\left[K_{W(B)}\alpha + k_{W(B)}\delta\right](\alpha + \delta) + \left[K_{B(W)}\alpha + k_{B(W)}\delta\right]\alpha + K_N\left(\frac{\alpha^2}{2}\right)\right\}\left(C_{L_\alpha}\right)_W + \left(\frac{A_p}{S_B}\right)c_{d_c}\,\overline{\eta}\left|\frac{\alpha_{D_{min}}}{57.3}\right|^3 \qquad (4)$$

where, for the wing-body combination tested,

$$\alpha_{D_{min}} = \frac{\delta}{|\delta|}\left[55 - \sqrt{(55)^2 + 86\,\delta\left(\frac{\delta}{|\delta|}\right)}\right] \qquad (5)$$

These equations were taken from reference 3 and converted to the notation of this report. The theory assumes that there is no leading-edge suction on the wing and that the resultant force on the body nose acts at a rearward inclination of $\alpha/2$ from the vertical in accordance with slender-body theory. The final term of equation (4) accounts for the effect of body crossflow on minimum drag but does not affect the drag rise; it was shown in reference 3 that inclusion of this term resulted in better agreement between theory and experiment. According to equation (4) the drag curve is a parabola; hence, the rate of drag rise $(C_D - C_{D_{min}}) / (\alpha - \alpha_{D_{min}})^2$ is the same at all deflections. Experimental values of C_{D_o} from the current tests are used in equation (4) since the theory determines drag rise only. The various quantities required for substitution in equation (4) are listed in table I.

Hinge Moment and Wing Center of Pressure

In reference 1 the following equation was advanced for the hinge moment of a wing in the presence of a cylindrical body:

$$C_h = -\left\{ K_{W(B)}\left[\left(\frac{\bar{x}}{c_r}\right)_{W(B)\alpha} - \left(\frac{x}{c_r}\right)_H \right]\alpha + k_{W(B)}\left[\left(\frac{\bar{x}}{c_r}\right)_{W(B)\delta} - \left(\frac{x}{c_r}\right)_H \right]\delta \right\}\left(\frac{c_r}{\bar{c}}\right)\left(C_{L_\alpha}\right)_W \tag{6}$$

Equation (6) can be separated into its component parts: hinge moment due to angle of attack

$$\Delta C_h = - K_{W(B)}\left[\left(\frac{\bar{x}}{c_r}\right)_{W(B)\alpha} - \left(\frac{x}{c_r}\right)_H\right]\left(\frac{c_r}{\bar{c}}\right)\left(C_{L_\alpha}\right)_W \alpha \qquad (\delta \text{ constant}) \tag{7}$$

and hinge moment due to wing deflection

$$\Delta C_h = -k_{W(B)}\left[\left(\frac{\bar{x}}{c_r}\right)_{W(B)\delta} - \left(\frac{x}{c_r}\right)_H \right]\left(\frac{c_r}{\bar{c}}\right)\left(C_{L_\alpha}\right)_W \delta \qquad (\alpha \text{ constant}) \tag{8}$$

It was pointed out in reference 1 that if the theoretical values of $\left(\frac{\bar{x}}{c_r}\right)_{W(B)\alpha}$ and $\left(\frac{\bar{x}}{c_r}\right)_{W(B)\delta}$ were used in the foregoing equations, accurate values of the hinge-moment coefficient were usually not obtained. An empirical modification was suggested to improve the method: Instead of the substitution of $\left(\frac{\bar{x}}{c_r}\right)_{W(B)\alpha}$ and $\left(\frac{\bar{x}}{c_r}\right)_{W(B)\delta}$ as read from the design chart (fig. 4 of ref. 1) directly into equations (7) and (8), the chart values should first be revised by adding the difference between the experimental and theoretical center-of-pressure positions of the wing alone; that is,

$$\left(\frac{\bar{x}}{c_r}\right)_{W(B)\alpha} = \left[\left(\frac{\bar{x}}{c_r}\right)_{W(B)\alpha}\right]_{theo} + \left\{\left[\left(\frac{\bar{x}}{c_r}\right)_W\right]_{exp} - \left[\left(\frac{\bar{x}}{c_r}\right)_W\right]_{theo}\right\} \quad (\delta = 0^\circ) \tag{9}$$

$$\left(\frac{\bar{x}}{c_r}\right)_{W(B)\delta} = \left[\left(\frac{\bar{x}}{c_r}\right)_{W(B)\delta}\right]_{theo} + \left\{\left[\left(\frac{\bar{x}}{c_r}\right)_{W}\right]_{exp} - \left[\left(\frac{\bar{x}}{c_r}\right)_{W}\right]_{theo}\right\} \qquad (\alpha = 0^\circ) \quad (10)$$

For the purposes of this report, the values of experimental wing-alone center of pressure were obtained from the data of reference 2 and converted to the notation used herein. The values are given in table I along with the various other parameters required for the preceding equations.

EXPERIMENTAL CONSIDERATIONS

Apparatus

Wind tunnel.- The tests were performed in the Ames supersonic wind tunnel No. 1 which has a test section nominally 1 foot wide by 3 feet deep. This wind tunnel is a continuous-operation, closed-circuit tunnel in which both the Mach number and the Reynolds number can be varied. During force tests, the humidity of the tunnel air is kept sufficiently low so that the effects of condensation of water vapor in the supersonic nozzle are negligible.

Balance system.- A four-component, strain-gage type of balance system, shown in figure 2(a), was used to measure the aerodynamic forces. The hinge moments were measured by means of a strain-gage beam enclosed within the body of the model. Two different types of balance support were used in the present investigation. For the $M = 1.46$ tests, the model and balance system rotated about a horizontal axis behind the balance (see fig. 2(a)); the maximum possible angle range with this support was only about -6° to $+6^\circ$. The support employed for the $M = 1.99$ tests rotated the model-balance system approximately about the midpoint of the model body; an angular range of about -20° to $+20^\circ$ was possible with this support.

Model.- The model used in this investigation consisted of a body and an all-movable wing which were fabricated from steel. Dimensional data are given in figure 2(b) and table II, and the model is shown mounted in the tunnel in figure 2(c). As can be seen in figure 2(a), the shafts of each wing panel (these panels are independent of each other) were supported by ball bearings in the sides of the body, and their ends were clamped together and held by friction in one end of the gage beam. The other end of the gage beam was restrained by the body structure. Deflection angles were set by means of jigs which slipped over the body and had angular cuts that fitted against one surface of each wing panel.

Sting.- The model was supported on the end of a tapered sting which was attached to the balance beam. Axes of the model and sting were coincident. For the $M = 1.46$ tests, two stings were used in order to extend the angle-of-attack range of the model. One sting had its axis coincident with that of the balance and was used for testing at angles of attack between about $\pm 6^\circ$. The other sting had its axis at approximately 7° relative to that of the balance; hence, the angle of attack could be varied from about 1° to around 14°. For the tests at $M = 1.99$, only the 7° sting was used.

The portion of the sting between the base of the model and the end of the balance was surrounded by a shroud, the purpose of which was to shield that part of the sting from the air stream. There was a gap of approximately 1/32 inch (in the no-load condition) between the base of the model and the nose of the shroud to allow for drag-gage deflection.

Tests and Methods

At a Mach number of 1.46 lift, drag, and hinge-moment data were obtained for ranges of angles of attack, wing deflection, Reynolds number, and wing-body gap. Most of the tests were run with natural transition of the boundary layer; for a few conditions, however, transition was fixed on the nose of the body. Only hinge-moment data were obtained at $M = 1.99$. All tests were run at zero yaw and zero bank. The scope of the test program is shown in detail in table III.

Angles of attack were determined from photographs which showed the position of the model relative to a wire-grid system affixed to the tunnel. For those runs listed as "transition fixed" in table III, two 0.010-inch-diameter wires were attached to the model about 1/4 inch and 3/8 inch (2- and 4-percent body length) from the body nose.

The drag data are presented in terms of foredrag, that is, total drag minus base drag, and all further references to drag in this report mean foredrag unless stated otherwise. Base drag was calculated from base-pressure measurements made concurrently with the force measurements. The base pressure was measured by an orifice which was located in the sting in the gap between the base of body and the nose of the shroud.

Precision of the Results

Calculations were made to determine the precision of the data presented in this report. In addition, a considerable number of check runs (21 percent) were made to ascertain the reliability of the instrumentation

and testing technique used. A study of the data showed that the precision calculations and check runs indicated errors of approximately the same order of magnitude. The precision of the data is summarized in the following table:

Item	Precision
M	± 0.01
C_L	± 0.04
C_D	± 0.02
C_h	± 0.002
α	$\pm 0.1^\circ$
g	± 0.003 in.
Model dimensions	± 0.02 in.

No corrections to the data for the effects of nonuniformities (stream angles and pressure gradients) in the test air stream were required.

Some comments concerning the wing settings are in order. The jigs used in setting the wings were machined to the nominal deflection angles within close tolerances. However, there was a systematic error in the settings; the left wing angle was always greater, and the right wing always less, than the nominal angle by about $1/4^\circ$ on the average. Even though a differential angle existed, the precision of the average deflection angle of the two wing panels relative to the nominal angles given in this report is about $\pm 0.1^\circ$.

RESULTS AND DISCUSSION

The lift, drag, and hinge-moment data obtained at $M = 1.46$ and $R = 5.7$ million with the small wing-body gap and transition natural are contained in figure 3. Figure 4 presents the hinge-moment data obtained at $M = 1.99$.

Lift

Effects of α and δ.- As shown in figure 3, the lift curves for all deflections are essentially linear at moderate angles of attack. If the lift data of figure 3 are replotted against the total angle of attack of the wing $\alpha + \delta$, then an upper limit of linearity is found to exist; it is approximately 8° for all the angle combinations of these tests. Above this angle there is a gradual decrease in lift curve slope with

increasing angle of attack and increasing deflection, the decrease due to δ being greater than that due to α. Maximum lift was not reached in these tests, even at $\alpha + \delta \approx 31^\circ$.

Comparisons with theory.- Theoretical lift is plotted in figure 3 along with the experimental data. In the angle-of-attack range where the experimental lift curves are linear, it is seen that the prediction of lift-curve slope (eq. (2)) is good at small values of $\alpha + \delta$. Beyond the linear range of the experimental data, where the limits of the theory have been exceeded, the slope prediction is poor. The C_L displacement between the experimental and theoretical lift curves, to be noted in the linear range of the experimental data, exists because the theory for the lift-curve slope due to deflection (eq. (3)) is not as accurate as the theory for the lift-curve slope due to angle of attack (eq. (2)) - this fact was also shown in figure 8 of reference 1.

Relative effectiveness.- The relative effectiveness of the wing in lift, η, is defined, for the purposes of this report, as the ratio of experimental lift to theoretical lift for the wing-body combination. In the region of zero lift, slopes were used in computing η, and the experimental curve for $\delta = 0^\circ$ was shifted to pass through the origin. Figure 5 shows the variation of η for the all-movable, triangular wing-body combination. The relative effectiveness of this type of control is seen to be good throughout the angular range tested. The decrease in η due to angle of attack is independent of wing deflection and amounts to about 10 percent at $\alpha = 15^\circ$. The decrease due to deflection is considerably greater and approximately linear, within the accuracy of the measurements. At low values of $\alpha + \delta$, the effectiveness is 98 percent; at $\alpha + \delta = 31^\circ$ it is 63 percent.

Effects of Reynolds number, fixing transition, and wing-body gap width.- Systematic tests were made to ascertain the effects of Reynolds number, fixing transition, and gap width on the aerodynamic characteristics. Presented in figure 6 are typical results from the tests that were conducted (table III). Figures 6(a), 6(b), and 6(c), respectively, show that Reynolds number, fixing transition, and gap had little or no effect on the lift data throughout the angular range tested. Variations in C_L of the order of ± 0.1 were considered small. The gap data presented in reference 1 for four values of gap width at only one Reynolds number and at zero deflection also showed little effect on lift.

Drag

Effects of α and δ.- Drag coefficient is plotted against angle of attack for various wing deflections in figure 3, where it can be seen that

the curves are essentially of parabolic shape. If the drag data of figure 3 are cross-plotted against δ for constant α and compared with the comparable data of figure 3 (see fig. 7 for typical results), it is apparent that the variation of $C_D - C_{D_{min}}$ with δ is only about half as much as the variation with α; this difference is predicted by theory. The increase in $C_{D_{min}}$ due to deflection is small as shown by the data (fig. 3) up to $\delta = 8^\circ$ and by the trends of the curves for $\delta = 12^\circ$ and 16°. The slight asymmetry of the drag curves is believed to be due to small stream effects.

Comparisons with theory.- The theoretical variation of drag, as given by equation (4), is plotted in figures 3 and 8 for comparison with the experimental data. Where the range of the data is such that the drag curves of figure 3 can be superimposed at $C_{D_{min}}$ and $\alpha_{D_{min}}$, the drag rise with increasing angle of attack, and consequently with lift, is found to be independent of deflection as predicted by theory (see eq. (4) and fig. 8 for sample results). For equal values of lift, the drag rise is the same for any combination of $\alpha + \delta$. The deviation that appears in the high angle-of-attack range of figure 8 is to be expected since the lift curves are nonlinear above $\alpha + \delta \approx 8^\circ$. In figure 3, at small deflections, theory gives a good prediction of the drag coefficient throughout the angle-of-attack range. As δ increases, theory overpredicts the magnitude of the drag. Although it may appear that the deviation, shown in figure 3, between theory and experiment is due entirely to the inaccurate prediction of the drag rise, in reality the inaccuracies in predicting $C_{D_{min}}$ and $\alpha_{D_{min}}$ contribute a major part of the deviation (this is clearly shown in fig. 8).

Effects of Reynolds number, fixing transition, and wing-body gap width.- The systematic tests made to determine the effects of Reynolds number, transition, and gap (table III), as discussed earlier in connection with lift, also included drag. Typical results are presented in figure 9. It was found that the effects of Reynolds number, transition, and gap were small or negligible. Variations in C_D of the order of ± 0.05 were considered small.

Hinge Moment and Wing Center of Pressure

The hinge-moment data obtained at $M = 1.46$ are presented in figure 3, and they are discussed in the following paragraphs.

Effects of α and δ.- Because the magnitude of the hinge moments is rather low, they have been plotted to a moderately large scale in figure 3. At $\delta = 0^\circ$, C_h is approximately zero throughout the angle-of-attack range. Positive deflection has the effect of lowering the over-all level of the

hinge-moment curves, C_h becoming increasingly negative with increasing deflection. For all deflections tested, except $\delta = 0^\circ$, the hinge-moment variation with angle of attack is nonlinear.

Wing center of pressure.- As the aerodynamic effects are not completely specified by the hinge-moment coefficient alone, wing center-of-pressure position has been plotted in figure 10, wherein the center of pressure has been computed from the relation

$$\frac{\bar{x}-x_H}{\bar{c}} = -\frac{C_h}{(C_L)_{W(B)}} = -\frac{C_h}{\eta\left[K_{W(B)}\alpha + k_{W(B)}\delta\right]\left(C_{L_\alpha}\right)_W} \tag{11}$$

The value of η for the wing-body combination (fig. 5) was used; this involved the assumption that the relative effectiveness of the exposed wing panels in the presence of the body is approximately the same as that of the wing-body combination.

The good balance characteristics of a triangular, all-movable wing control at $M = 1.46$ throughout the angular range are indicated by figure 10. At $\delta = 0^\circ$, the particular control arrangement tested is balanced at all angles of attack. For all $\alpha > 1\text{-}1/2^\circ$, the wing center of pressure moves aft with increasing deflection, but, even at $\delta = 16^\circ$, it is within about 3-percent $\bar{c}$ of the hinge line. At any constant δ, the center-of-pressure shift is not more than about 2-percent $\bar{c}$ at positive angles of attack.

Comparisons with theory.- For direct comparison, the theoretical hinge moment given by equation (6) has been plotted in figure 3, and the theoretical center-of-pressure positions given by equations (9) and (10) have been plotted in figure 10. With regard to hinge moment, the agreement between theory and experiment in figure 3 is satisfactory in the low and moderate angle-of-attack range, where the theory is applicable, at all deflections tested. In the high α range, especially at the higher deflections where the experimental curves become decidedly nonlinear, the theory fails to predict the magnitude of the hinge moment.

With reference now to figure 10, it is seen that the modified theoretical prediction of the center-of-pressure position due to angle of attack at $\delta = 0^\circ$ is almost within 1-percent $\bar{c}$ of that obtained by experiment, which is within the accuracy limits of both experiment and theory. Theory gives a rearward shift in the center of pressure due to deflection at $\alpha = 0^\circ$ of about 2-1/2-percent $\bar{c}$ which is almost exactly equal to the shift found by experiment. Also shown in figure 10 are the unmodified theoretical center-of-pressure positions given directly by the chart of reference 1. The values are about 6-percent $\bar{c}$ aft of the

values given by experiment; thus, the modification to the theory used herein is justified for this particular wing-body combination.

Effects of Reynolds number, fixing transition, and wing-body gap width.- The tests (table III), discussed earlier, made to determine the effects of Reynolds number, fixing transition, and gap on lift also included hinge moment. A study of the results (sample shown in fig. 11) revealed that the effects of Reynolds number and fixing transition were small or negligible. Variations in C_h of the order of ± 0.01 are considered small. Some effect of gap is shown in the vicinity of $\alpha \approx 8°$; the effect is not considered large, however, since the magnitude of the hinge moment is small due to the close balance of the control.

Effects of Mach number.- Hinge-moment data at $M = 1.99$ are presented in figure 4. It is to be noted that the hinge-moment curves have the same general shape at all deflections: The curves are nearly linear (average slope $C_{h_\alpha} \approx -0.002/\text{deg}$) up to a total angle $\alpha + \delta$ of about 25°, at larger total angles they are also essentially linear at a greatly increased slope (average $C_{h_\alpha} \approx -0.023/\text{deg}$). This increased slope appears to be due to a rearward shift of the center of pressure. The trend of the theoretical hinge moment at $M = 1.99$ is, in general, similar to that computed at $M = 1.46$; consequently, the results are not plotted in figure 4.

Experimental hinge-moment data at Mach numbers of 1.46 and 1.99 are compared directly in figure 12 for deflections of 0° and 16°. Mach number is seen to have little or no effect on C_h at angles of attack below 6°. The trends of the curves are noticeably different at higher angles of attack.

CONCLUSIONS

The following conclusions have been reached from a study of the results of systematic tests of a triangular all-movable wing and body configuration:

1. The relative effectiveness, defined as the ratio of experimental lift to theoretical lift, was between 63 and 98 percent throughout the angle-of-attack and deflection range tested. The theory of NACA RM A52D29 was adequate for the prediction of the lift variation in the low $\alpha + \delta$ range to which it applies.

2. For equal values of lift, the drag rise was the same for any combination of $\alpha + \delta$; however, for equal angles the drag rise due to deflection was only about half that due to angle of attack. The increase in minimum drag due to deflection was small. The theory of NACA RM A52I30 was adequate for the prediction of drag only at small angles of attack and small deflections.

3. The wing as a control can be fairly closely balanced over a large α and δ range since the maximum center-of-pressure shift was only about 3 percent of the mean aerodynamic chord at positive angles of attack at $M = 1.46$. The method of NACA RM A52D29 for predicting hinge moment and center of pressure, as modified herein, gave fairly good agreement with experiment at $\alpha + \delta$ less than about 20° at $M = 1.46$.

4. Reynolds number variation, fixing transition at the body nose, and wing-body-gap width variation, over the range of variables tested, had little or no effect on lift, drag, or hinge moment at $M = 1.46$. The effects of Mach number on hinge moment were nil at low angles of attack.

Ames Aeronautical Laboratory
National Advisory Committee for Aeronautics
Moffett Field, Calif., June 22, 1953

REFERENCES

1. Nielsen, Jack N., Kaattari, George E., and Drake, William C.: Comparison between Prediction and Experiment for All-Movable Wing and Body Combinations at Supersonic Speeds - Lift, Pitching Moment, and Hinge Moment. NACA RM A52D29, 1952.

2. Nielsen, Jack N., Katzen, Elliott D., and Tang, Kenneth K.: Lift and Pitching-Moment Interference between a Pointed Cylindrical Body and Triangular Wings of Various Aspect Ratios at Mach Numbers of 1.50 and 2.02. NACA RM A50F06, 1950.

3. Katzen, Elliott D., and Pitts, William C.: Comparison between Prediction and Experiment for All-Movable Wing and Body Combinations at Supersonic Speeds - Drag Due to Lift and Lift-Drag Ratio. NACA RM A52I30, 1952.

4. Gowen, Forrest E., and Perkins, Edward W.: Drag of Circular Cylinders for a Wide Range of Reynolds Numbers and Mach Numbers. NACA TN 2960, 1953.

TABLE I.- VALUES OF PERTINENT PARAMETERS AT M = 1.46

$(C_{L_\alpha})_W$ (calculated from ref. 2)	0.291
K_N (ref. 1)	0.120
$K_{B(W)}$ (ref. 1)	0.275
$K_{W(B)}$ (ref. 1)	1.165
$k_{B(W)}$ (ref. 1)	0.221
$k_{W(B)}$ (ref. 1)	0.944
C_{L_α} (eq. (2))	0.454
C_{L_δ} (eq. (3))	0.339
c_{d_c} (ref. 4)	1.2
$\overline{\eta}$ (ref. 4)	0.685
$\left[(\overline{x}/c_r)_W\right]_{exp}$ (calculated from ref. 2)	0.620
$\left[(\overline{x}/c_r)_{W(B)\alpha}\right]_{theo}$ (ref. 1)	0.650
$\left[(\overline{x}/c_r)_{W(B)\delta}\right]_{theo}$ (ref. 1)	0.668
$\left[(\overline{x}/c_r)_W\right]_{theo}$	0.667
$(x/c_r)_H$ (fig. 2(a))	0.611
C_{h_α} (eq. (7))	0.0041
C_{h_δ} (eq. (8))	-0.0041

TABLE II.- MODEL DIMENSIONAL DATA

[The dimensions given below are design values; maximum deviations are not more than ±0.025 inch.]

Body	
Length	10.500 in.
Maximum diameter	1.125 in.
Fineness ratio	9.333
Base (and maximum cross-section) area	0.994 sq in.
Plan-form area	10.473 sq in.
Volume	8.83 cu in.
Nose length	3.188 in.
Nose shape	30° cone with an ogival transition section (tangent to cone and cylindrical afterbody)
Wing	
Span (no gap)	5.625 in.
Area	
Exposed panels joined together	5.062 sq in.
Total (leading edge and trailing edge extended to body axis)	7.912 sq in.
Maximum chord	
At body juncture	2.250 in.
At body axis (leading edge and trailing edge extended)	2.812 in.
Mean aerodynamic chord (exposed panels)	1.500 in.
Thickness ratio	0.08
Sweepback of leading edge	45°
Aspect ratio (exposed panels joined together)	4
Airfoil section	Symmetrical double wedge
Miscellaneous	
Reference moment center (aft of nose)	5.250 in.
Wing-body gap	
Normal	0.016 in.
Extended (for these tests)	0.062 in.

TABLE III.- SCOPE OF THE TEST PROGRAM

M	R x 10^{-6}	[1]α_{nom}, range deg	[2]δ_{nom}, deg	g/d	Transition
1.46	1.3	-6 to 6	-5,5	0.013	Natural
↓	1.3	1 to 13	0	0.057	↓
↓	2.8	-6 to 13	-5,0,2, 5,8,12,16	0.013	↓
↓	↓	-6 to 13	0,8	0.057	↓
↓	↓	0 to 13	12	0.057	↓
↓	↓	-6 to 6	-5,0,5	0.013	Fixed
↓	↓	↓	0	0.057	Fixed
↓	4.1	↓	-5,5	0.013	Natural
↓	4.1	1 to 13	0	0.057	↓
↓	5.7	-6 to 13	-5,0,2, 5,8,12,16	0.013	↓
↓	↓	-6 to 13	0,5,8	0.057	↓
↓	↓	0 to 13	12	0.057	↓
↓	↓	-6 to 6	-5,0,5	0.013	Fixed
↓	↓	-6 to 6	0	0.057	Fixed
1.99	5.8	-5 to 25	0,5,8, 12,16	0.013	Natural

[1]Excludes deflection due to bending of support system under load.
[2]All data are presented in terms of these nominal values.

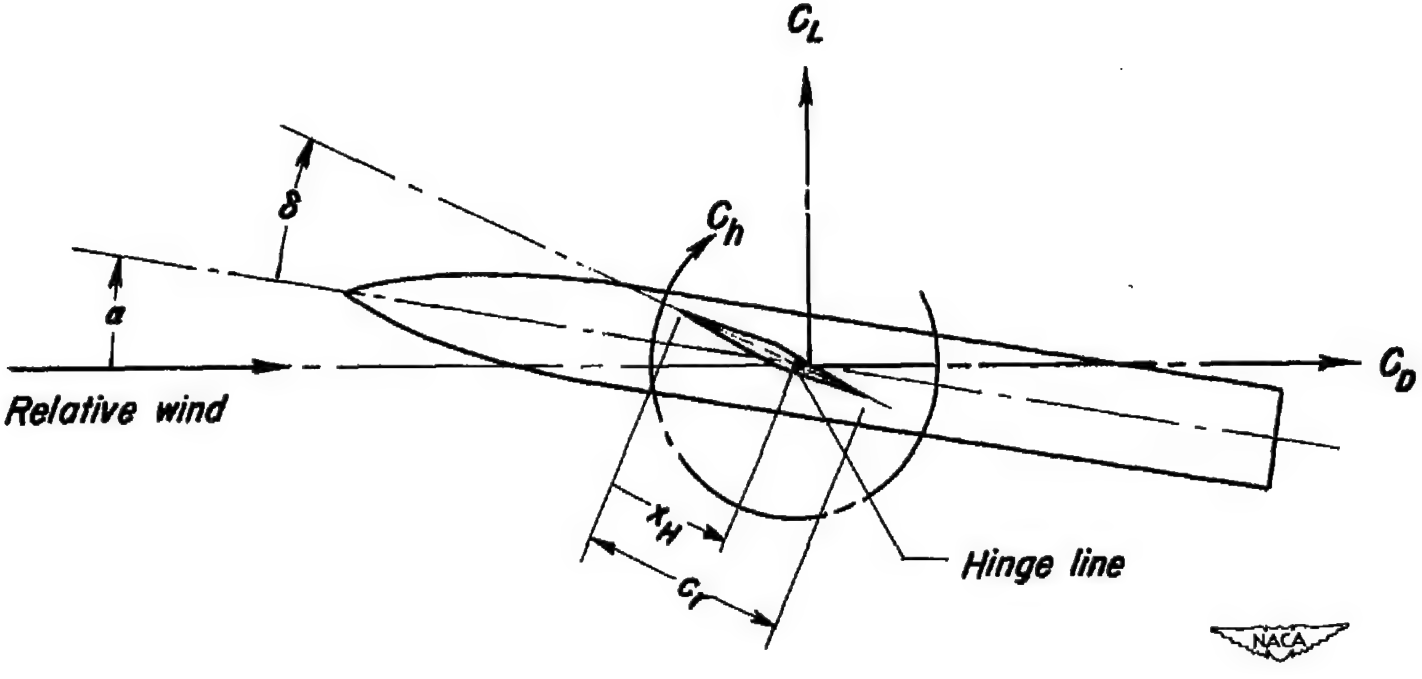

Figure 1. — Positive sense of all coefficients, angles, and directions.

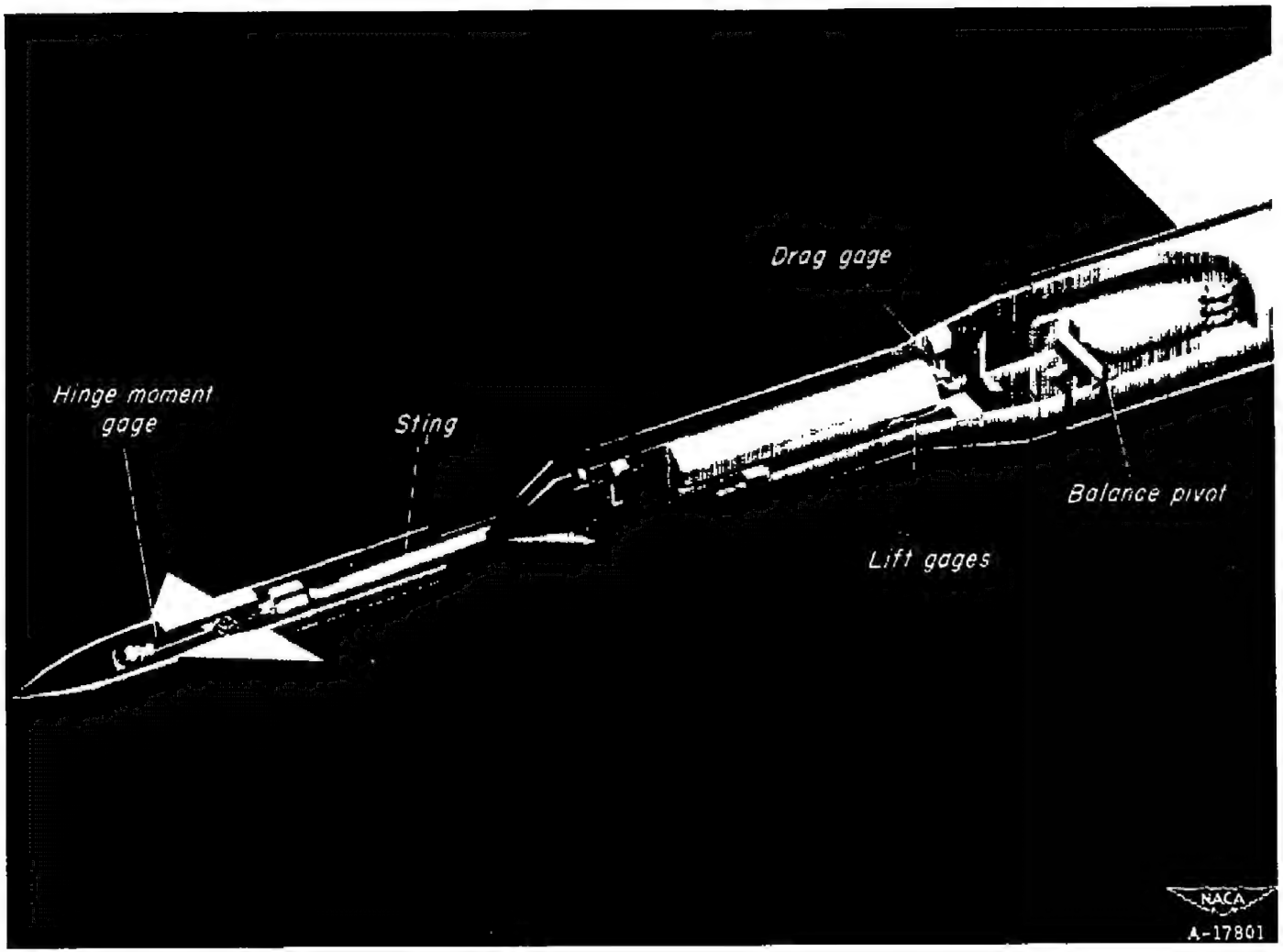

(a) Schematic diagram of model and strain-gage balance system.

Figure 2. - Model and balance system.

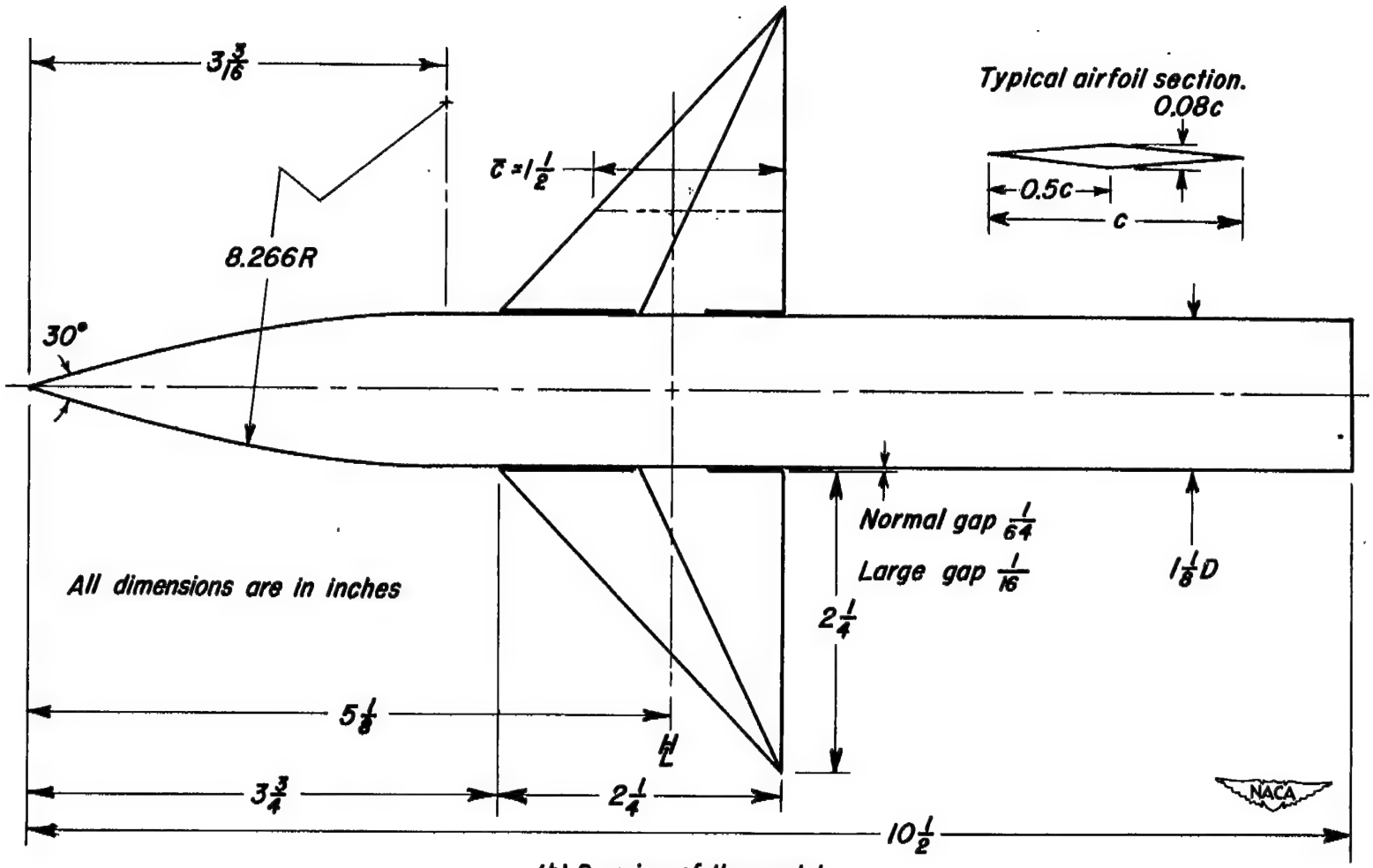

(b) Drawing of the model.

Figure 2.- Continued.

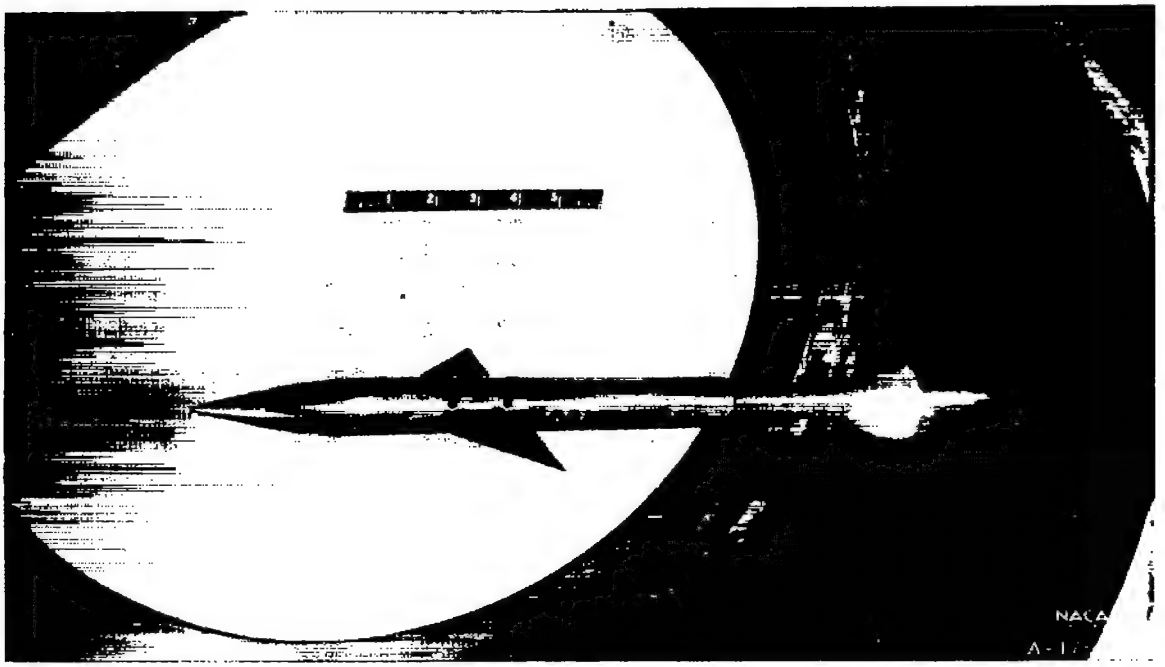

Model on 0° sting; $\delta = 0°$, balance at 0°

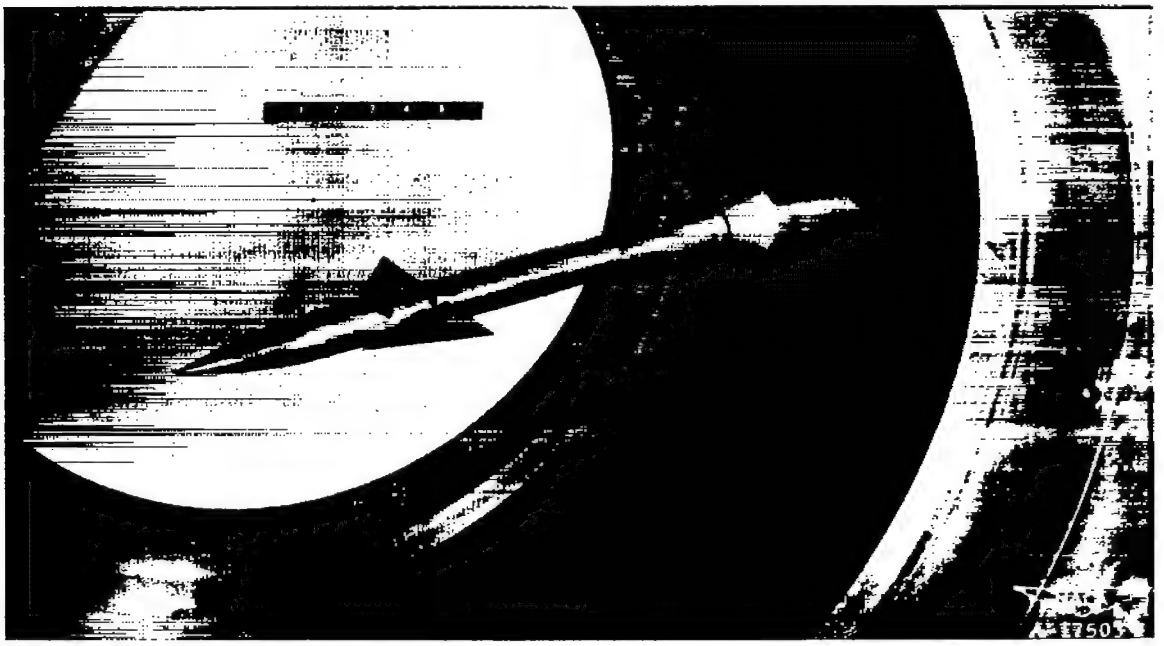

Model on 7° sting; $\delta = 16°$, balance at 0°

(c) Installation of model in tunnel.

Figure 2.- Concluded.

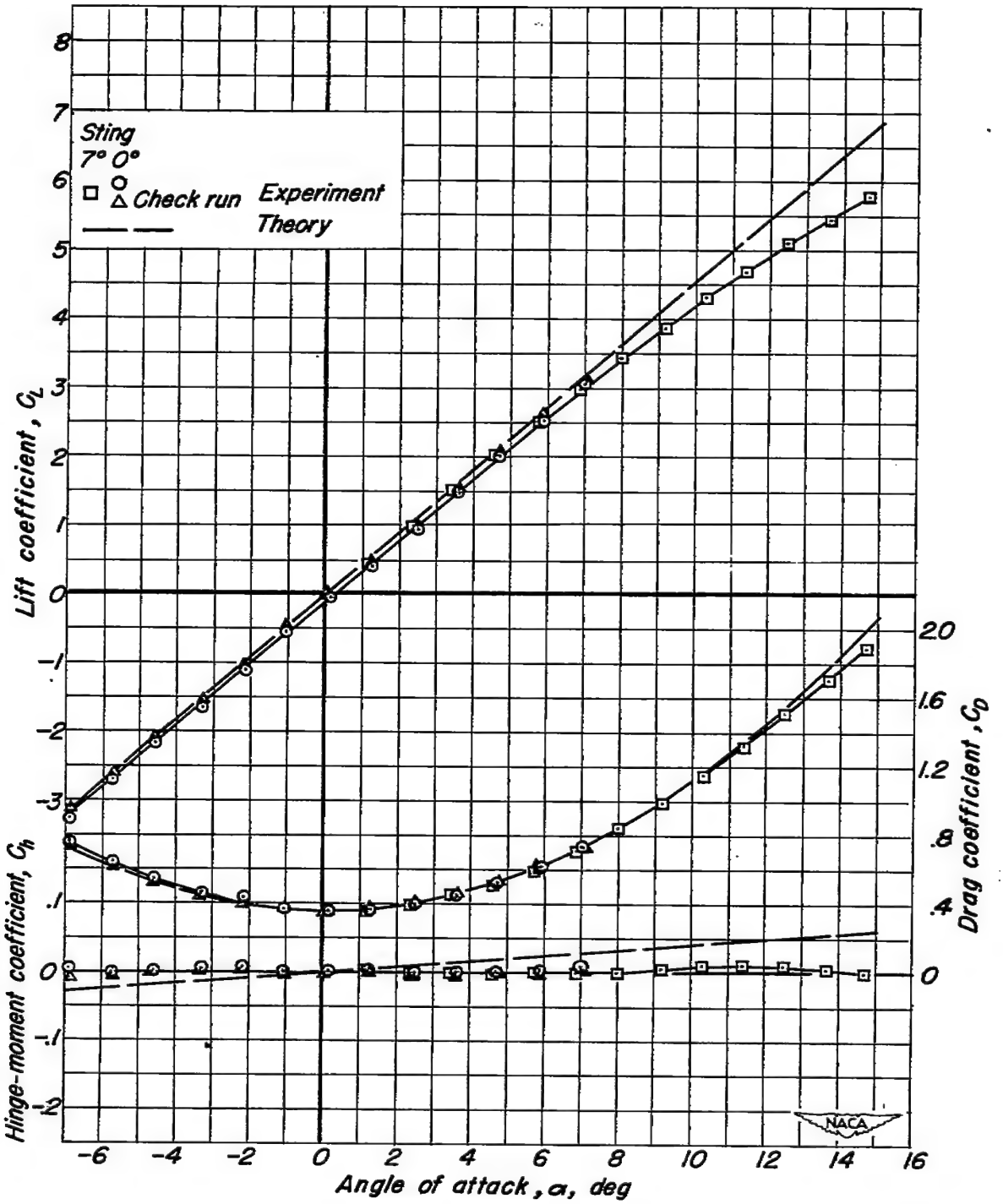

(a) $\delta = 0°$

Figure 3.— Aerodynamic characteristics of the wing-body combination. $M = 1.46$, $R = 5.7 \times 10^6$, $g/d = .013$, transition natural.

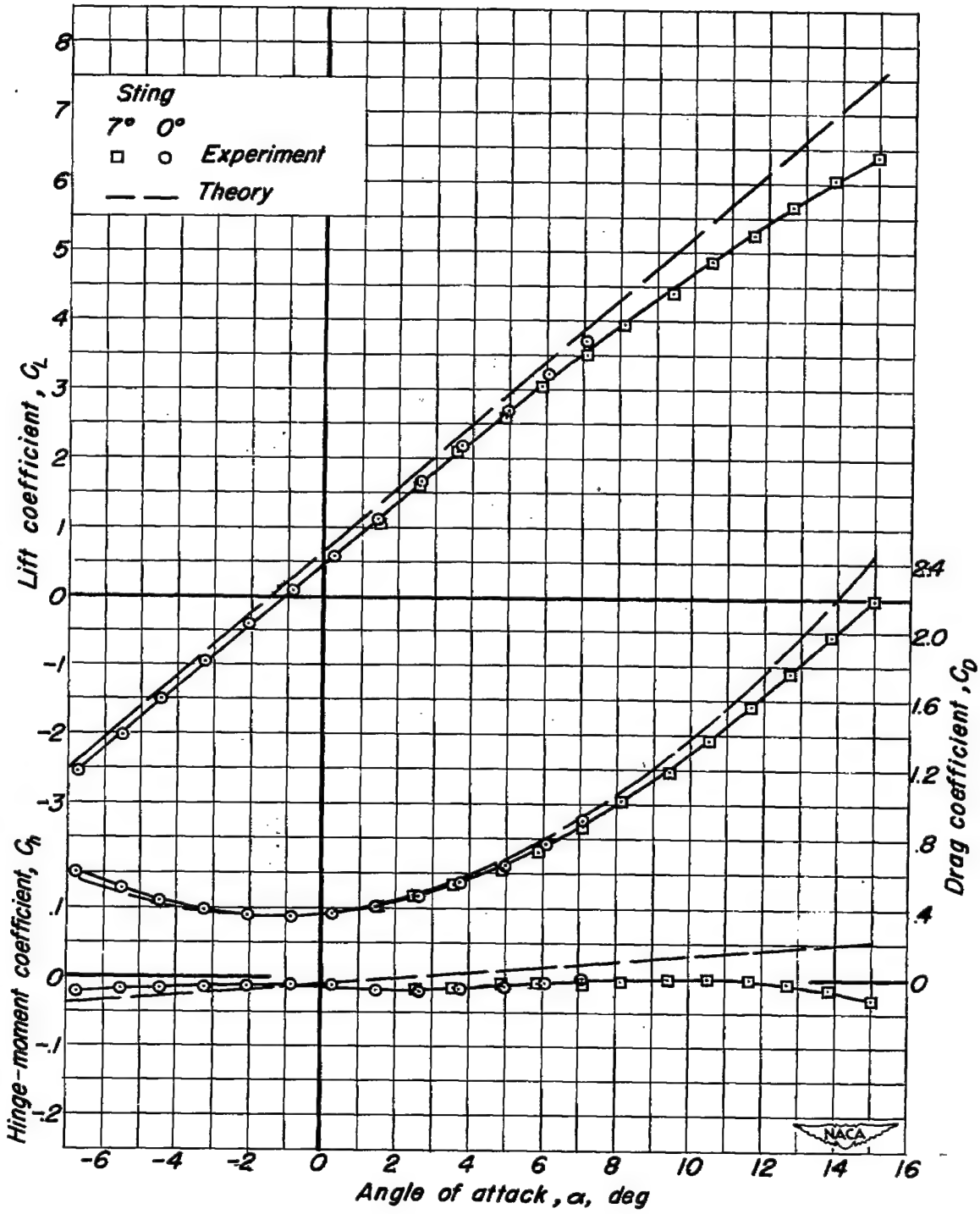

(b) $\delta = 2°$

Figure 3.— Continued.

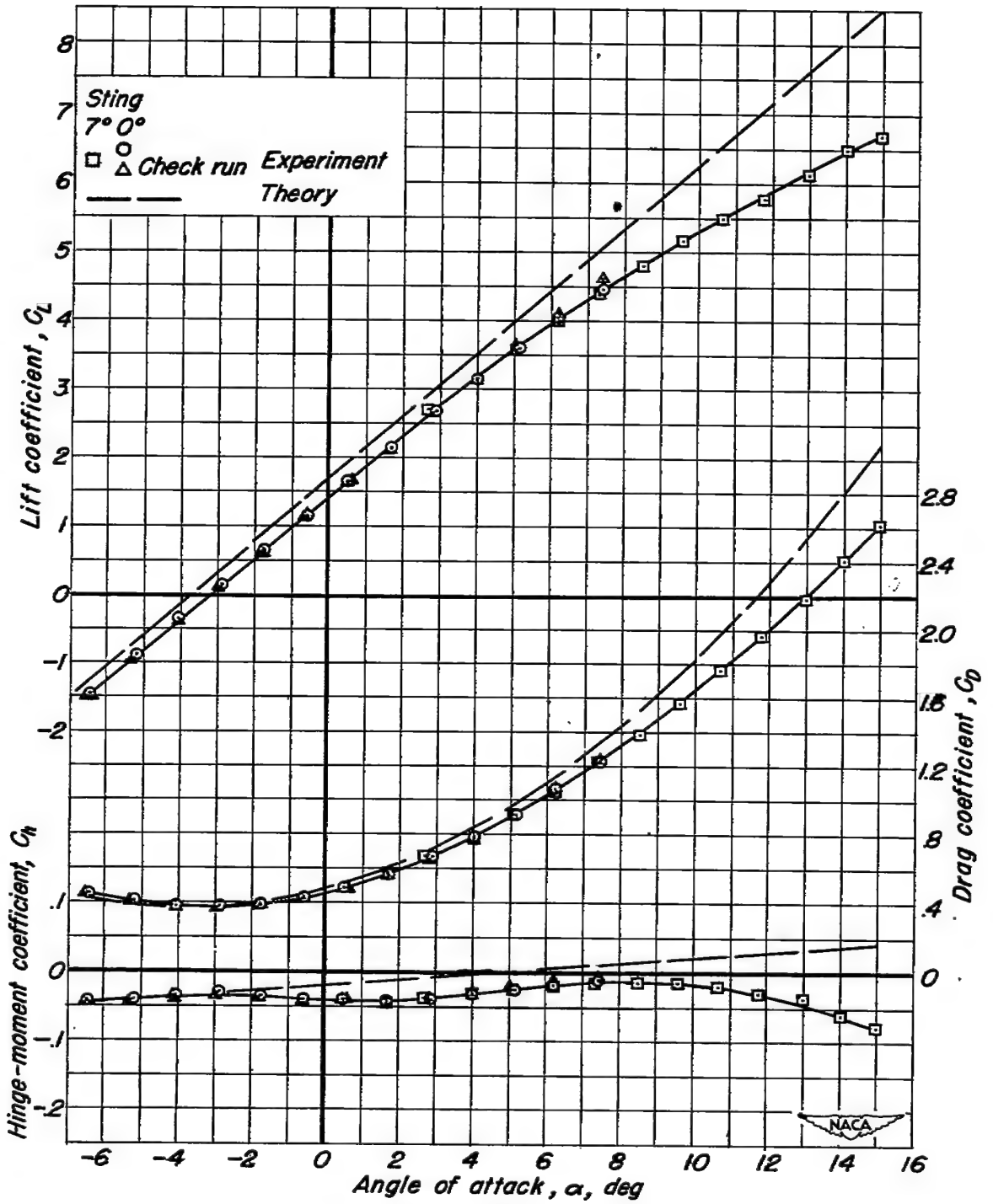

(c) $\delta = 5°$

Figure 3.- Continued.

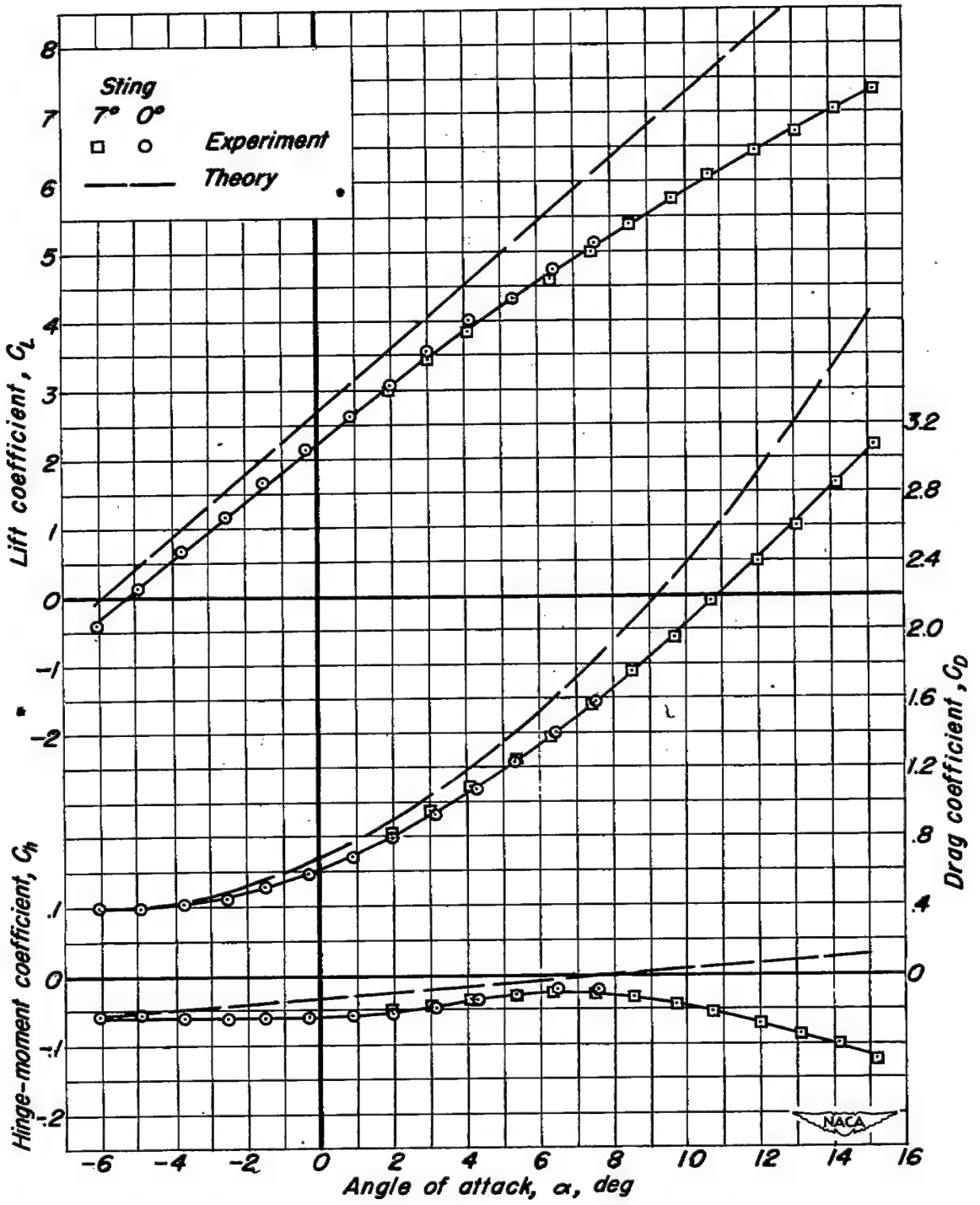

(d) $\delta = 8°$

Figure 3.– Continued.

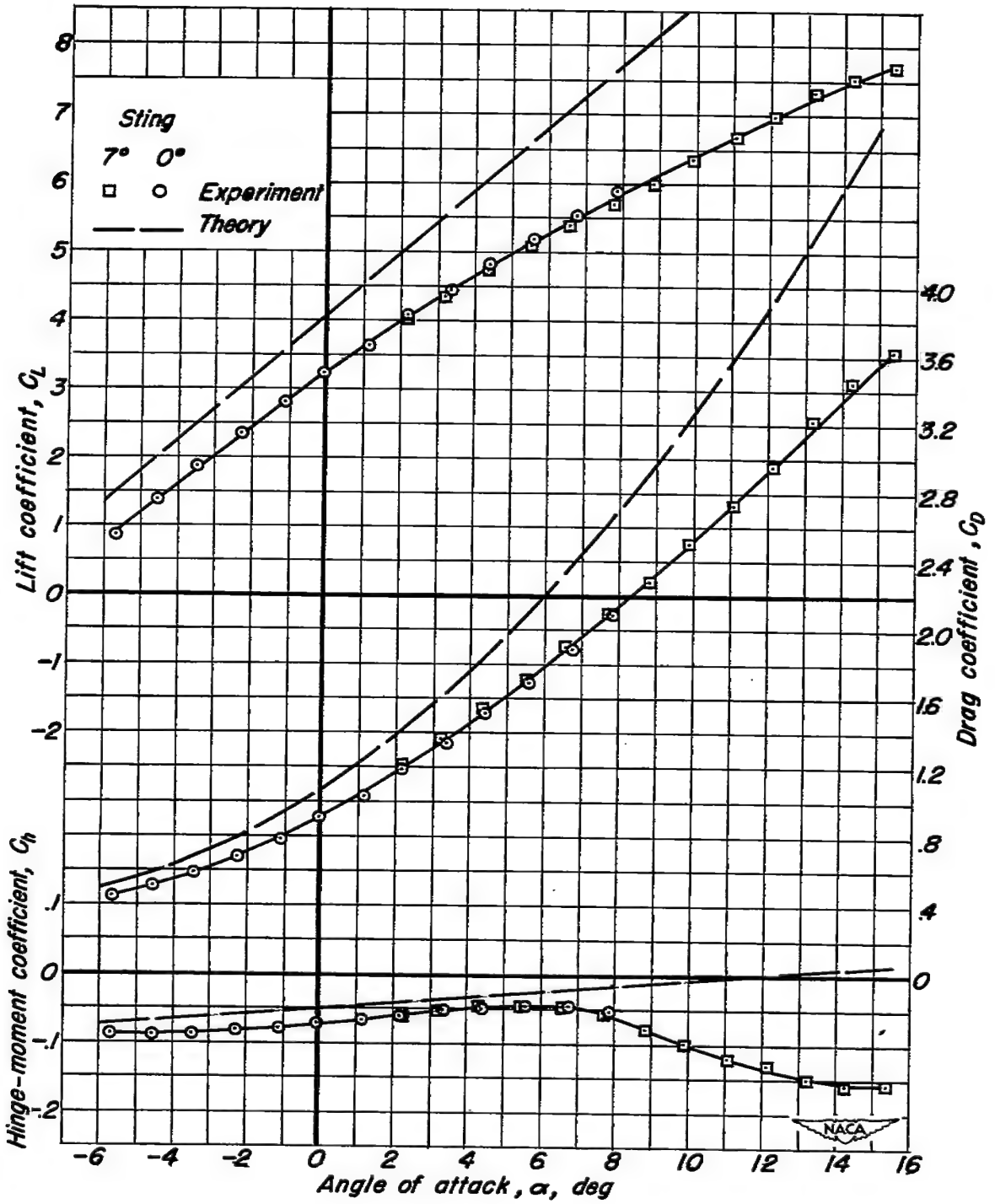

(e) $\delta = 12°$

Figure 3.- Continued.

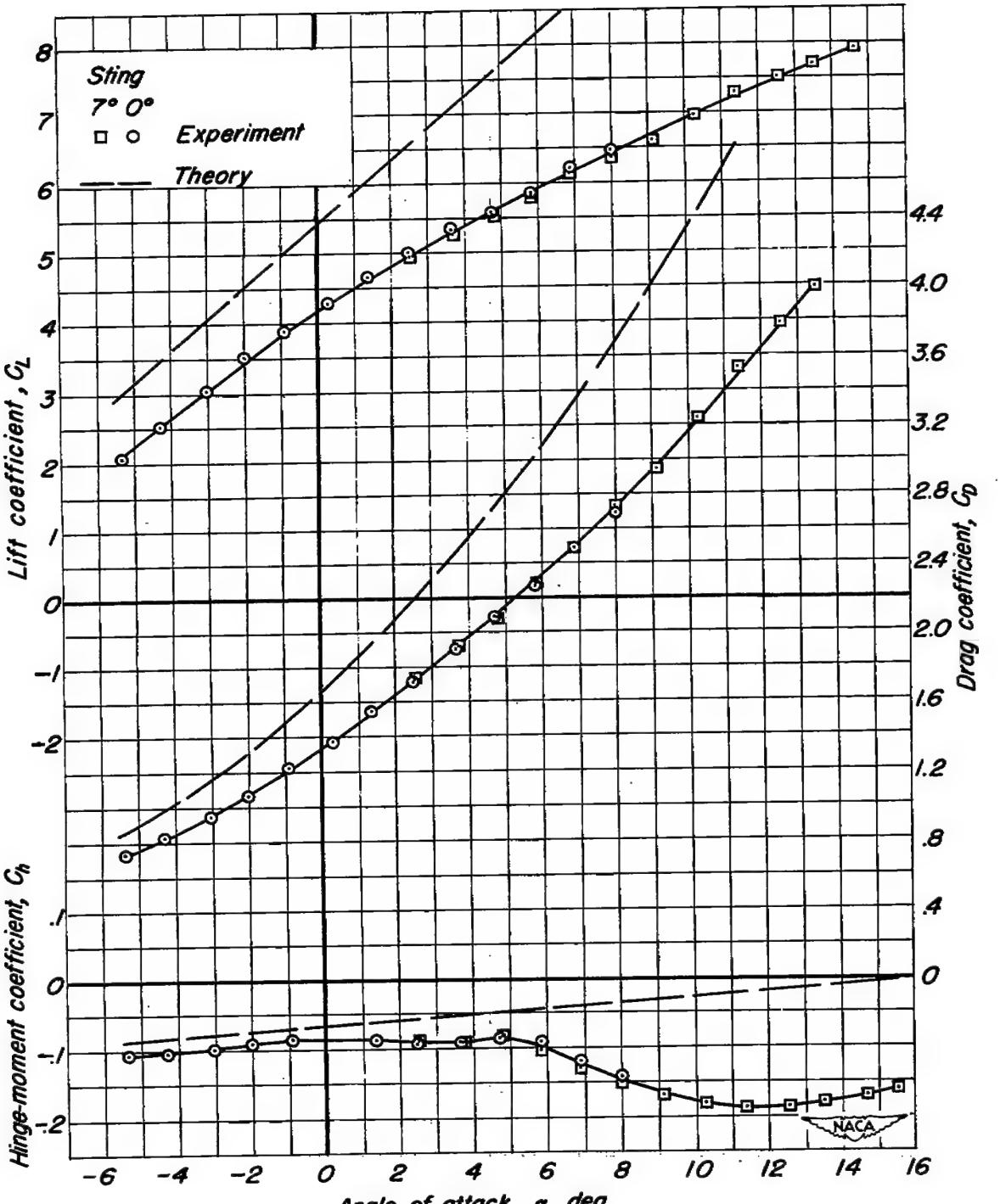

(f) $\delta = 16°$

Figure 3.– Continued.

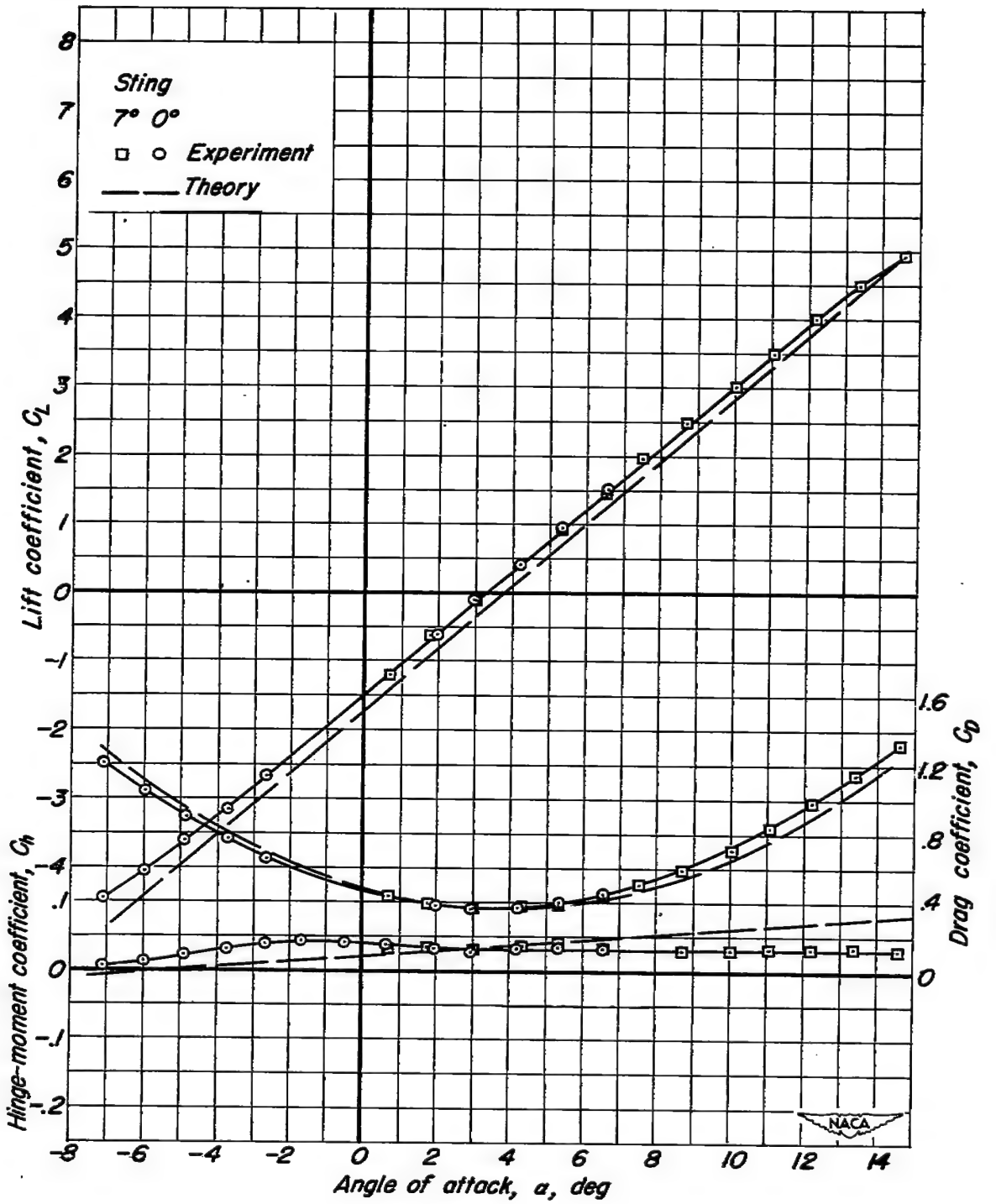

(g) $\delta = -5°$

Figure 3. – Concluded.

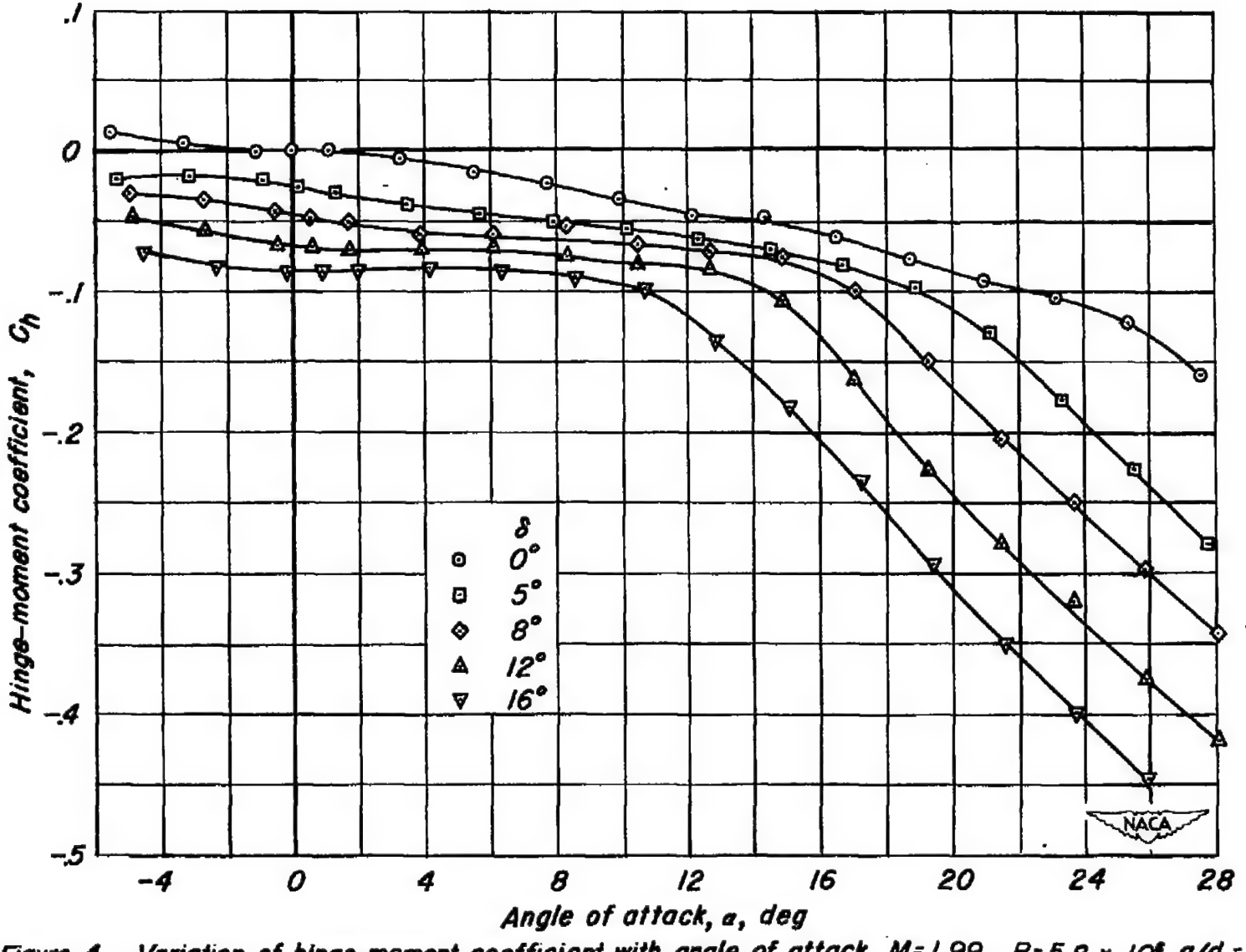

Figure 4.— Variation of hinge-moment coefficient with angle of attack. M = 1.99, R = 5.8 x 10^6, g/d = .013.

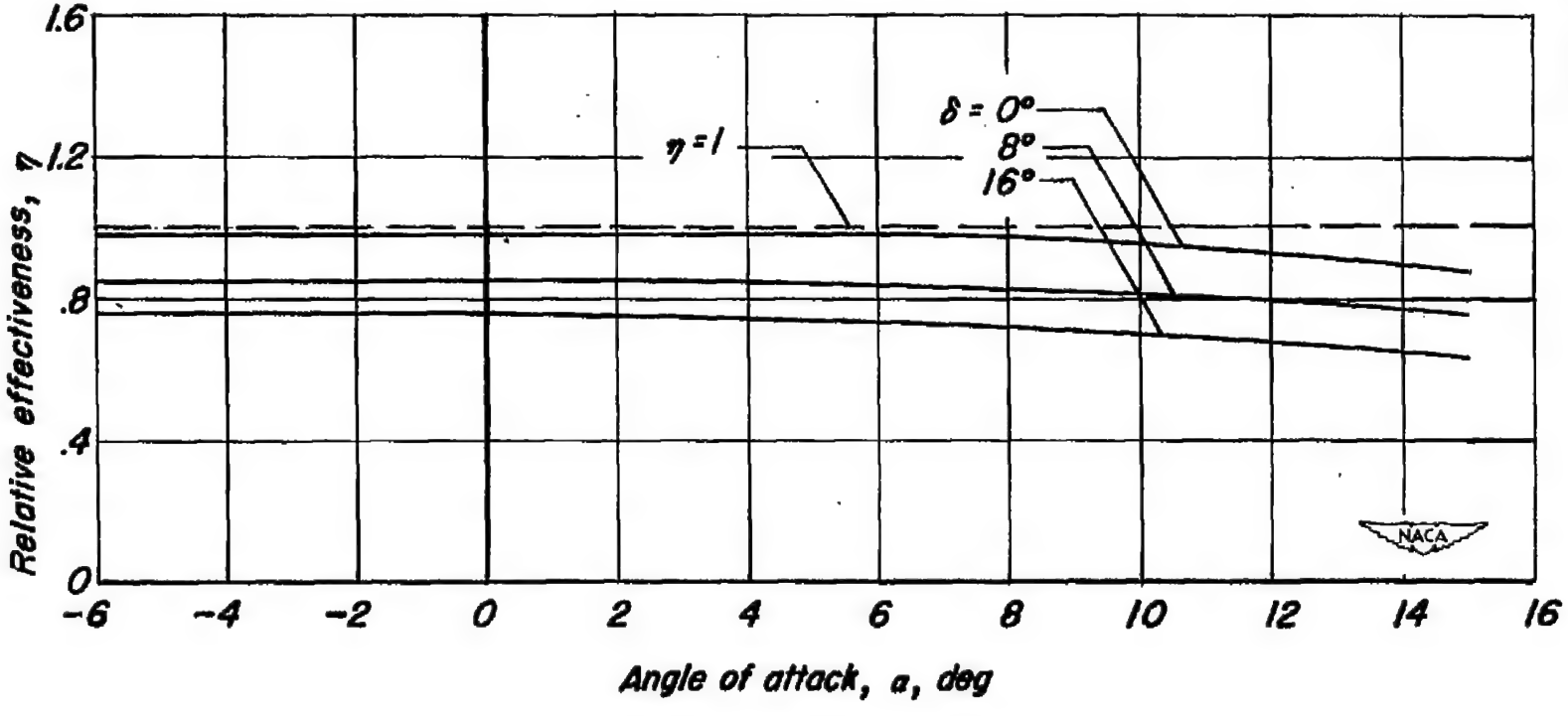

Figure 5.— Variation of relative effectiveness in lift with angle of attack. M=1.46, R=5.7 x 10⁶, g/d=.013.

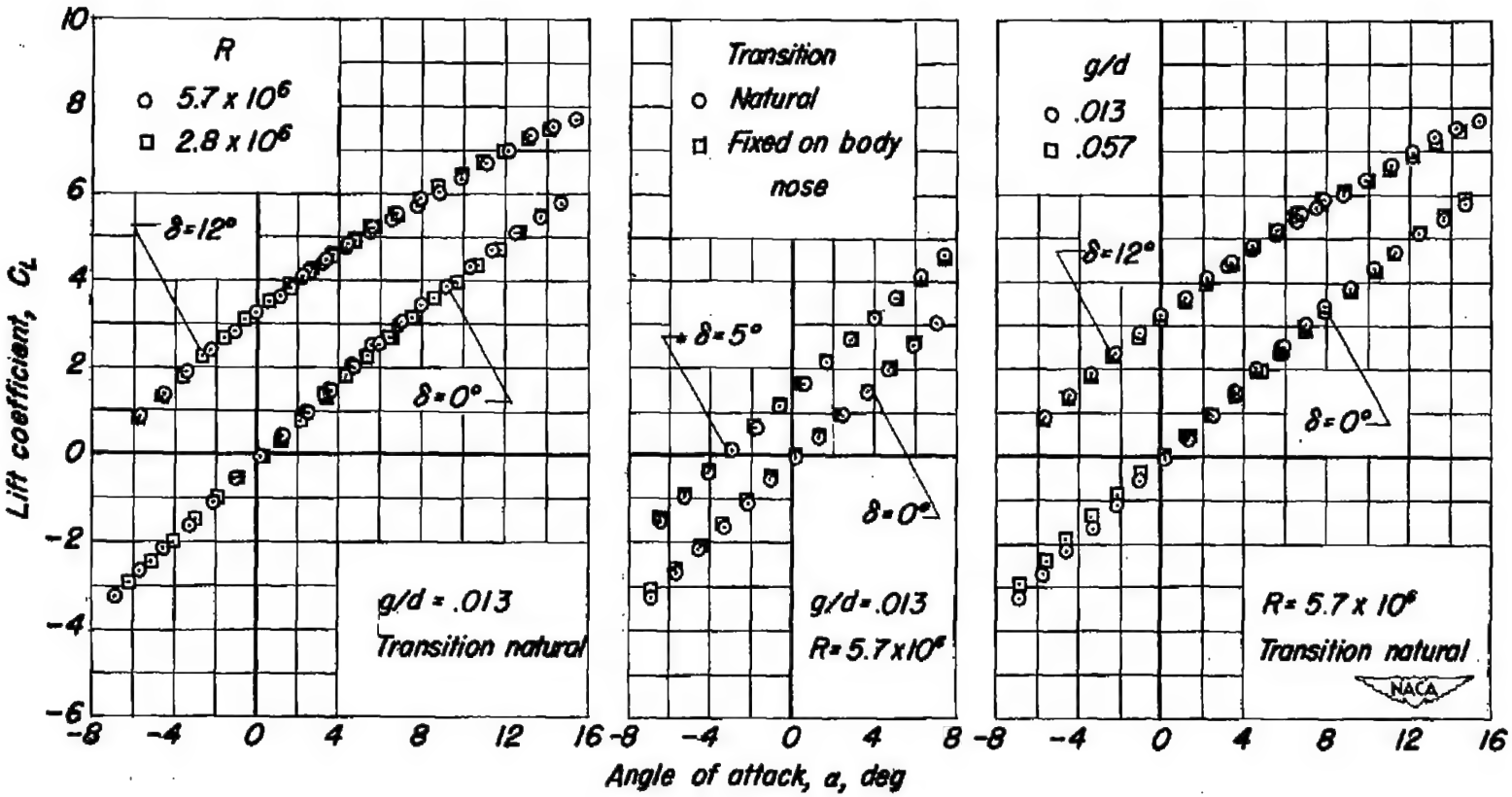

(a) Effect of Reynolds number. (b) Effect of transition. (c) Effect of gap.

Figure 6.– Effect on lift of Reynolds number, fixing transition, and wing-body gap. M = 1.46.

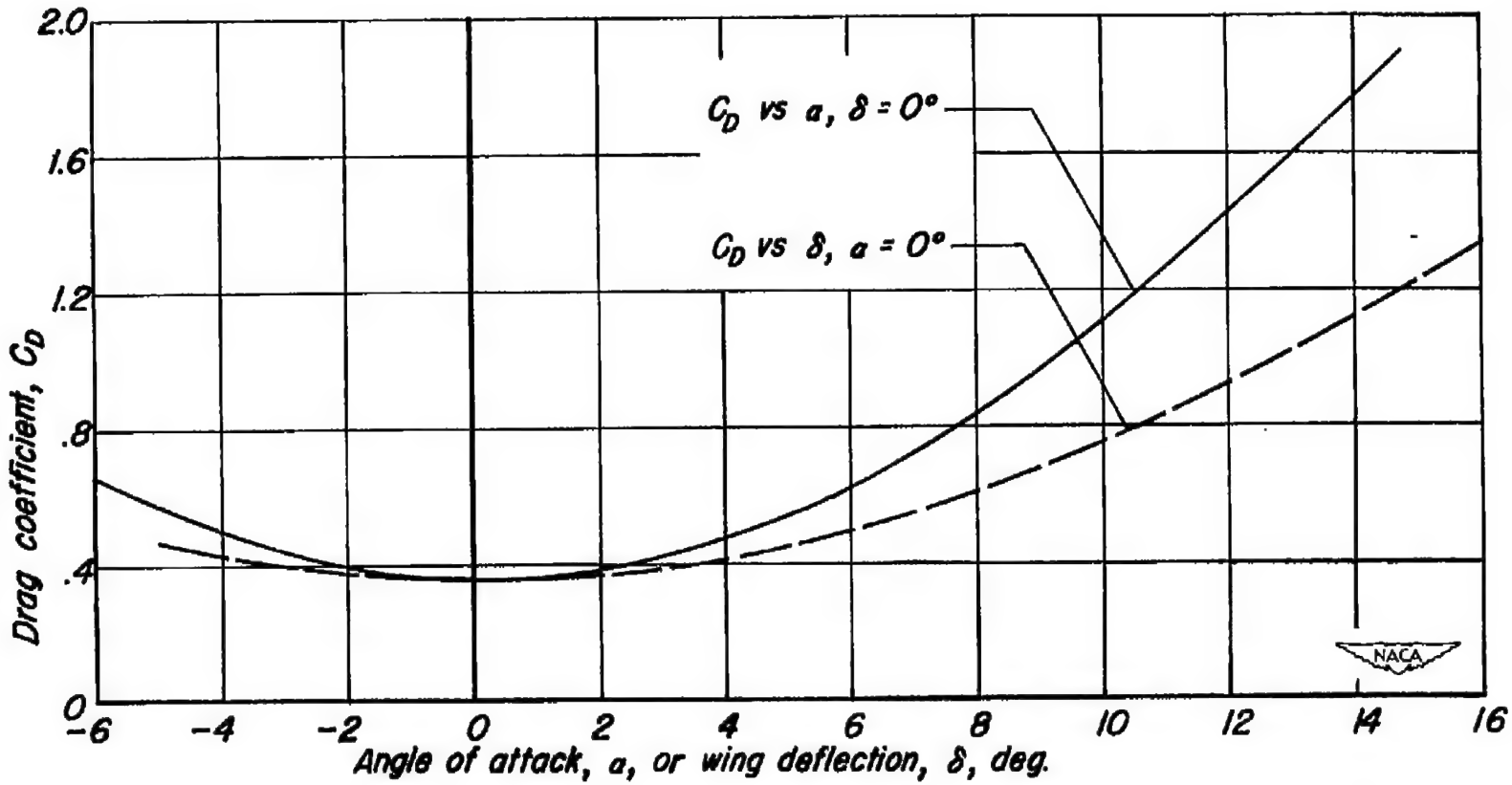

Figure 7.— Comparison of variation of drag coefficient with angle of attack and with wing deflection. M = 1.46, R = 5.7 x 10^6, g/d = .013.

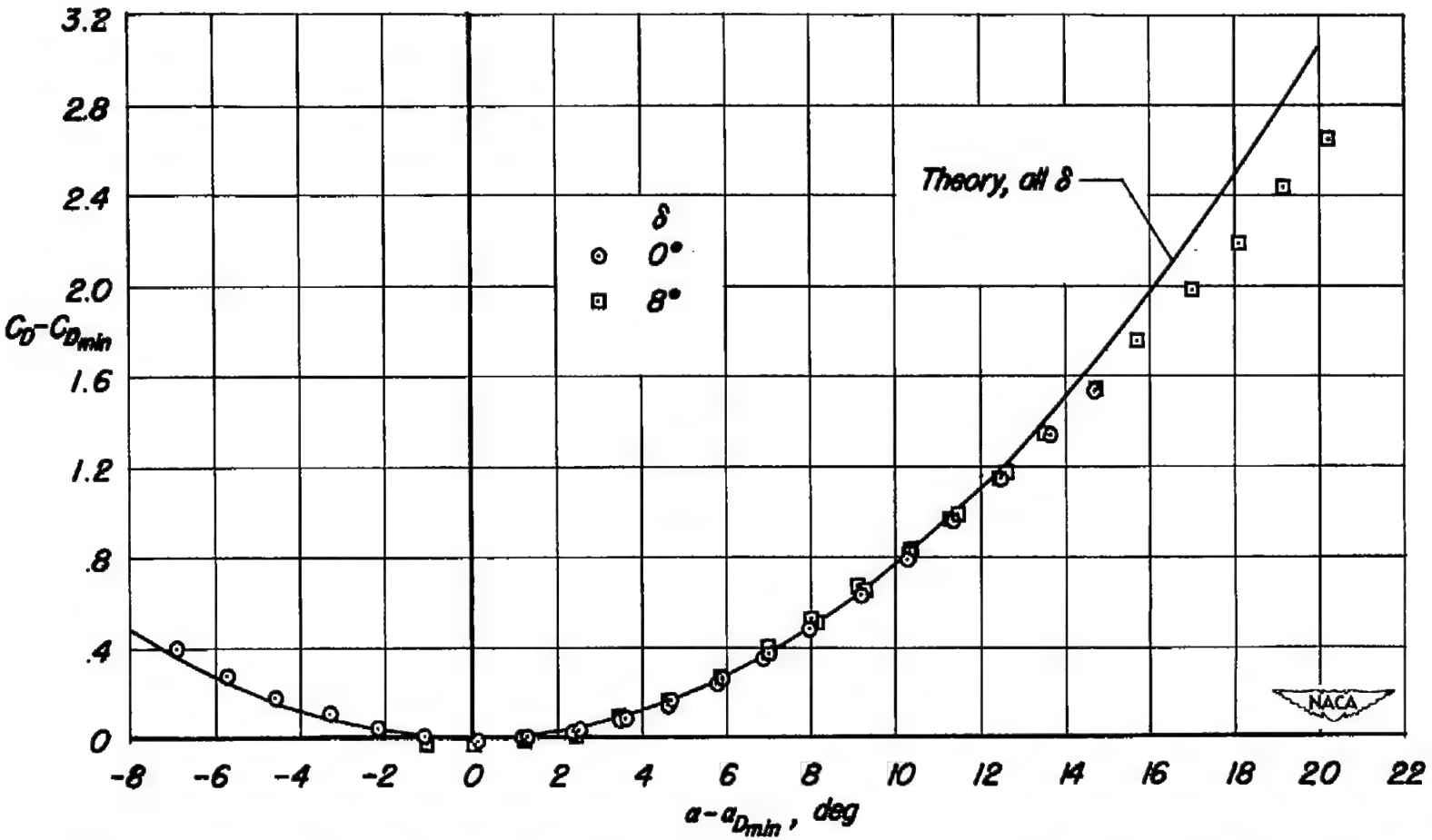

Figure 8.– Comparison of the drag due to lift at two deflections. M=1.46, R=5.7 x 10^6, g/d=.013.

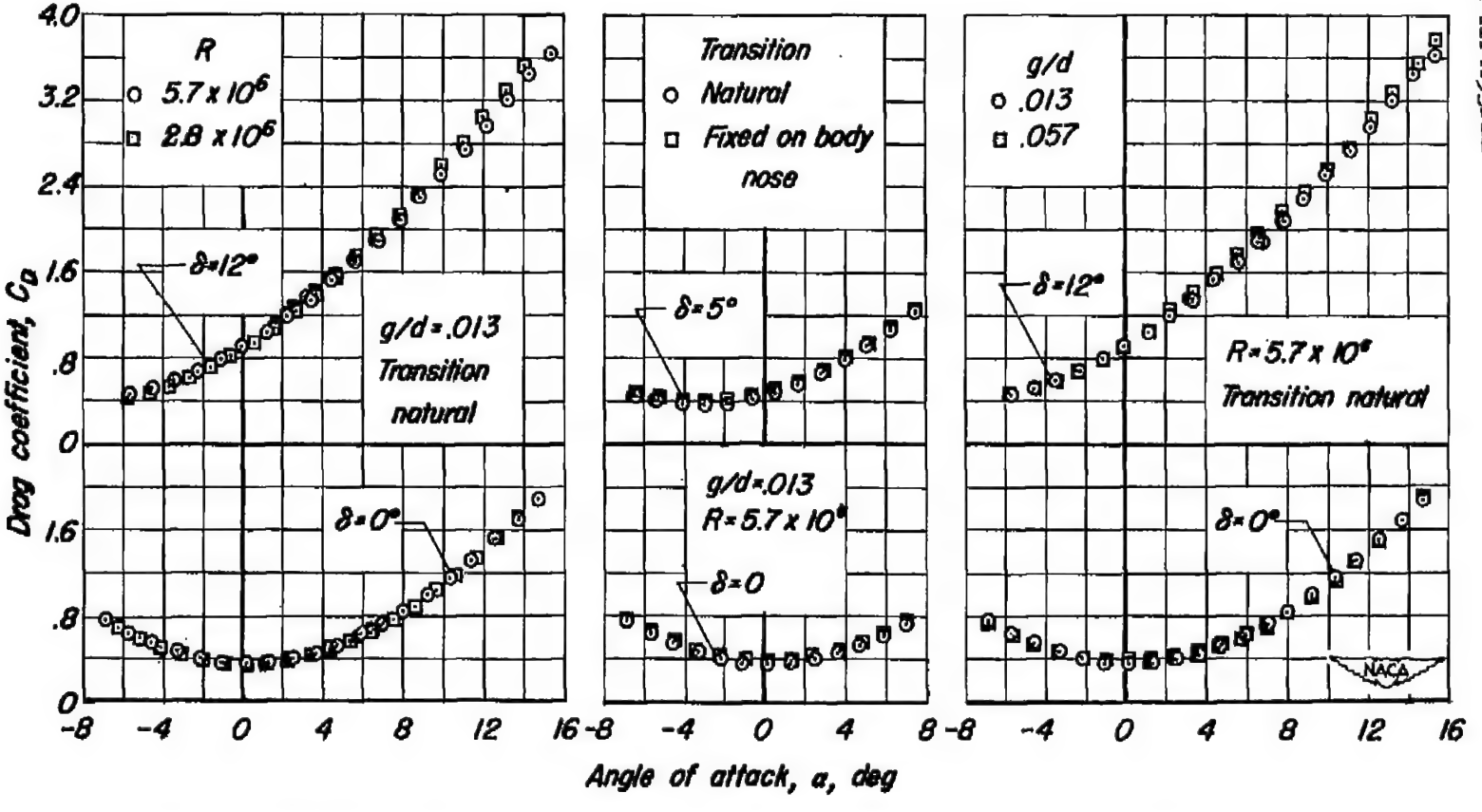

(a) Effect of Reynolds number. (b) Effect of transition. (c) Effect of gap.

Figure 9.– Effect on drag of Reynolds number, fixing transition, and wing-body gap. M=1.46.

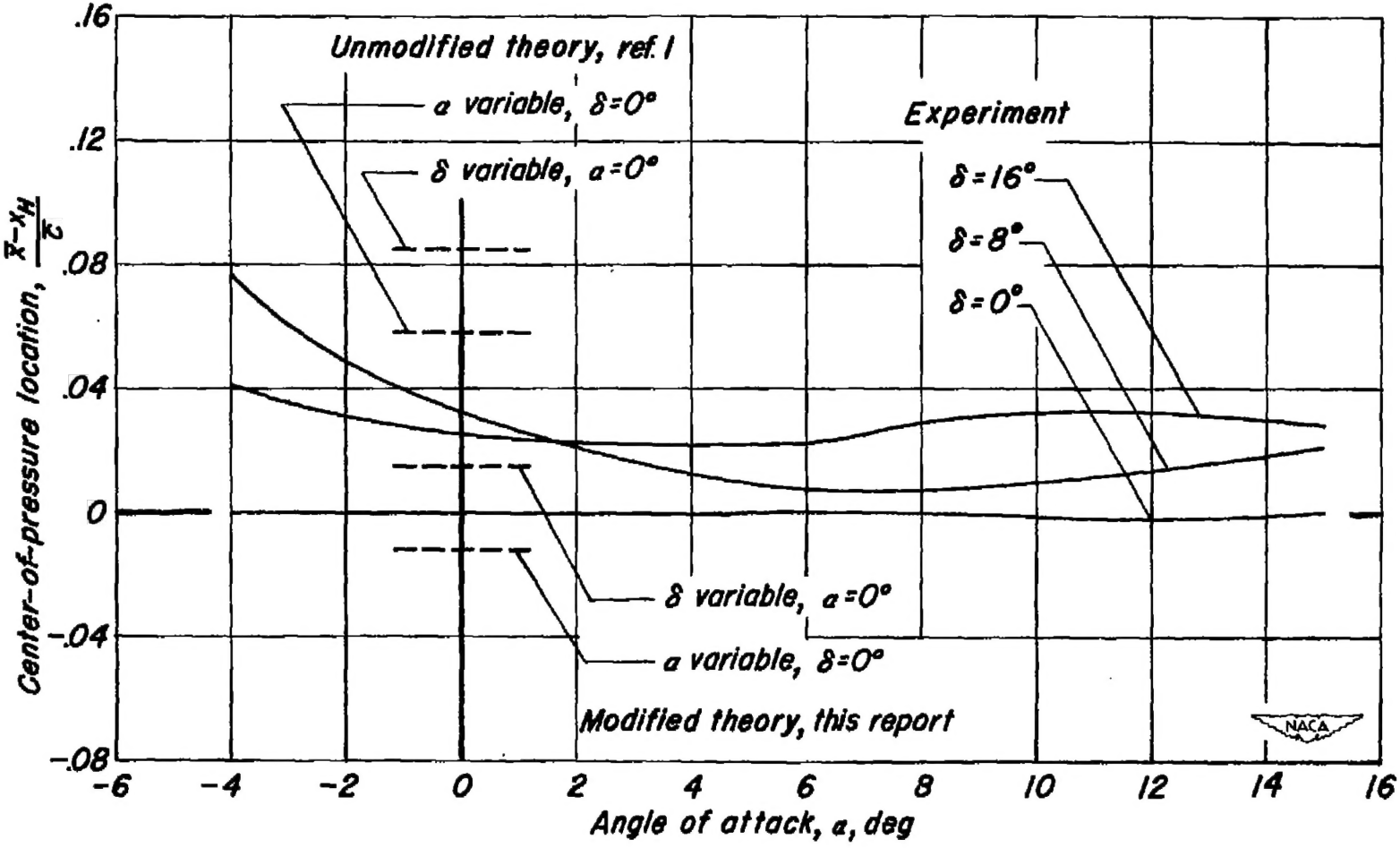

Figure 10.—Variation of wing center of pressure with angle of attack. M = 1.46, R = 5.7 x 10⁶, g/d = .013.

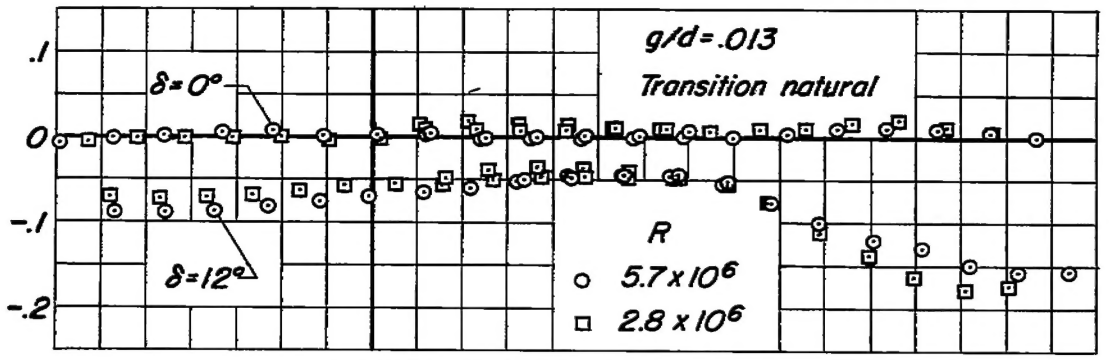

(a) Effect of Reynolds number.

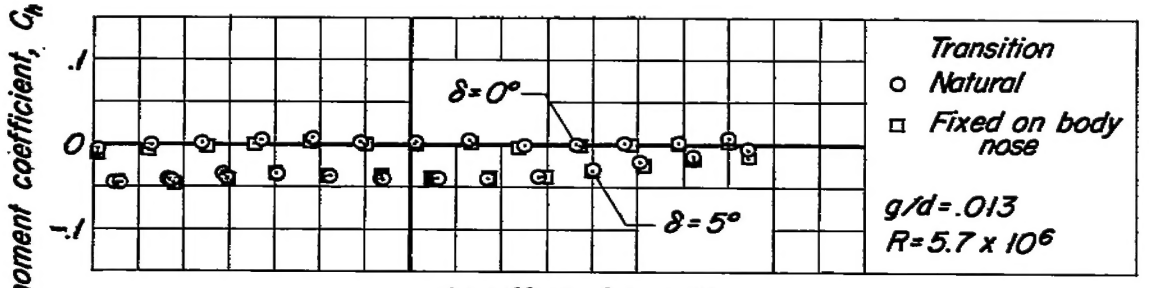

(b) Effect of transition.

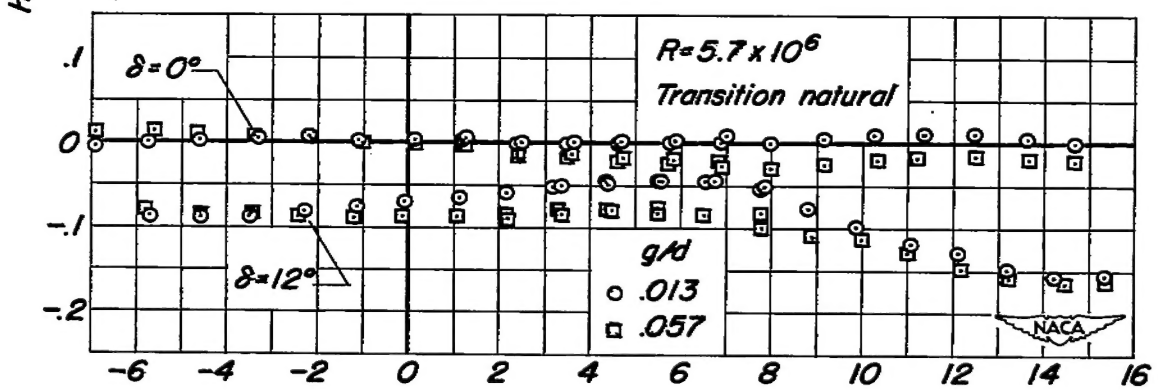

(c) Effect of gap.

Figure 11.— Effect on hinge moment of Reynolds number, fixing transition, and wing-body gap. M=1.46.

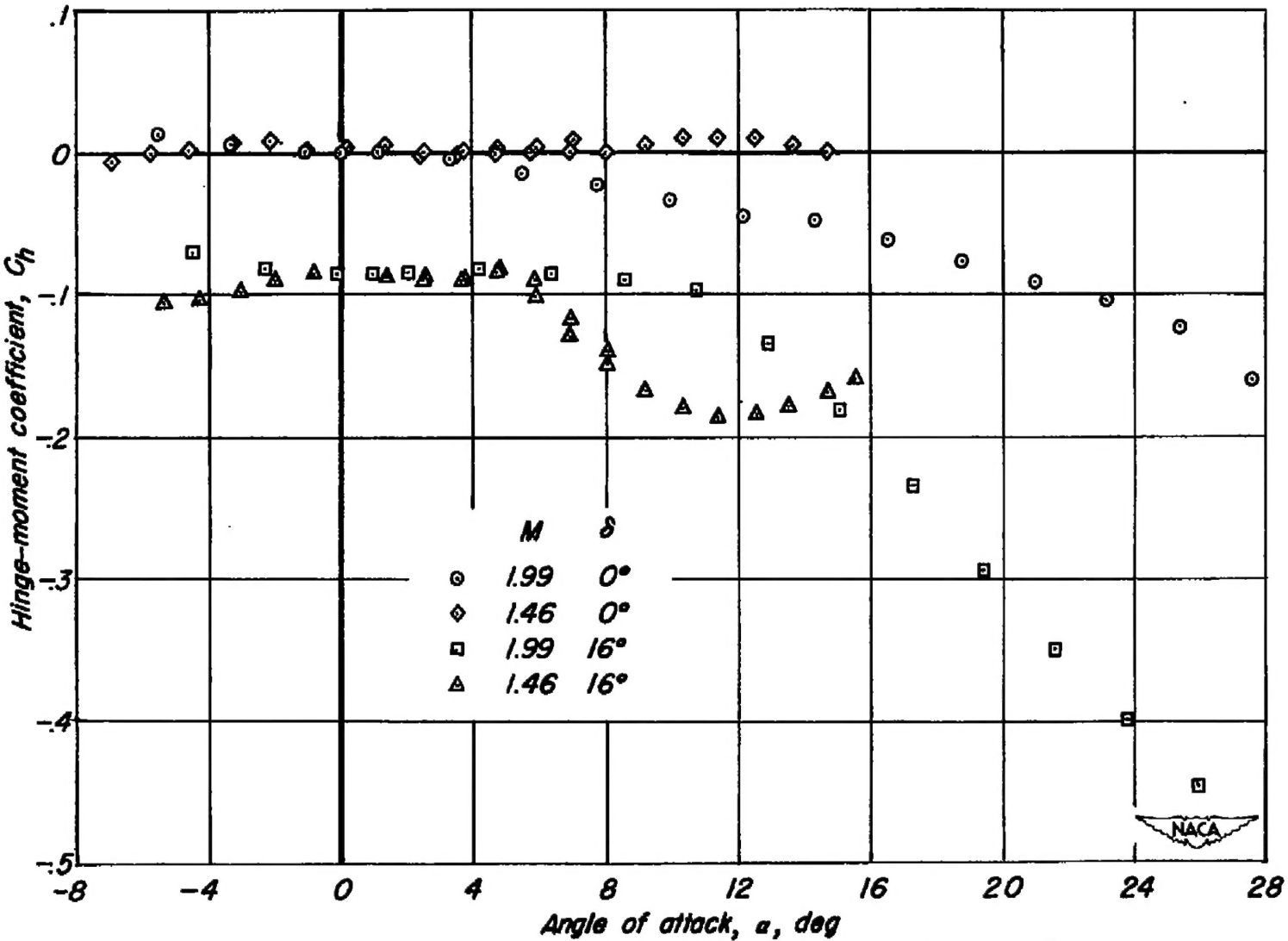

Figure 12. — Effects on hinge-moment coefficient of Mach number. $R=5.7 \times 10^6$; $g/d = .013$.